NASA CR-176972

A Reproduced Copy

OF

NASA-CR-176972
19860019681

N86-29153

Reproduced for NASA

by the

NASA Scientific and Technical Information Facility

FINAL REPORT

Covering Period March 1981 - September 1984

MEASUREMENT OF TEMPERATURE AND DENSITY FLUCTUATIONS IN TURBULENCE USING AN ULTRAVIOLET LASER

Grant NAG 2-104, NASA-Ames Research Center

The NASA Technical Officer for this grant is

Dr. Robert L. McKenzie

Principal Investigator: G. A. Massey

Institution: San Diego State University
San Diego, CA. 92182-0190
Department of Electrical and
Computer Engineering

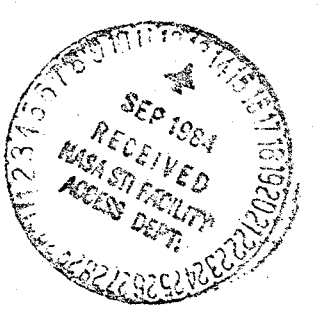

I. Introduction

This report summarizes research under grant NAG 2-104 from spring 1981 through summer 1984 on the topic of noninvasive measurement of density and temperature fluctuations in turbulent air flow. The approach that has been investigated uses fluorescence of oxygen molecules which are selectively excited by a tunable vacuum ultraviolet laser beam. The strength of the fluorescence signal and its dependence on laser wavelength vary with the density and temperature of the air in the laser beam. Because fluorescence can be detected at 90° from the beam propagation direction, spatial resolution in three dimensions, rather than path-integrated measurements, can be achieved. With spatial resolutions of the order of a millimeter and at supersonic air velocities it is necessary to perform each measurement in a time of the order of a microsecond; this is possible by using laser pulses of ten nanosecond duration.

In this method atmospheric O_2 is excited by the emission of a tunable ArF excimer laser, and the fluorescence, which spans the 210 - 420 range, is detected by an ultraviolet phototube. The ArF laser is tunable over the 193-194 nm range, which includes several rotational features of the Schumann-Runge absorption system of O_2. Figures 1 and 2 show the spectroscopic details of interest here. Since the ground state rotational level fractional populations are affected by temperature, and the total number of O_2 molecules in the observation volume depends on the density of the air, there is the possibility of simultaneous determination of both temperature and density. Originally, we planned to use non-specific excitation with

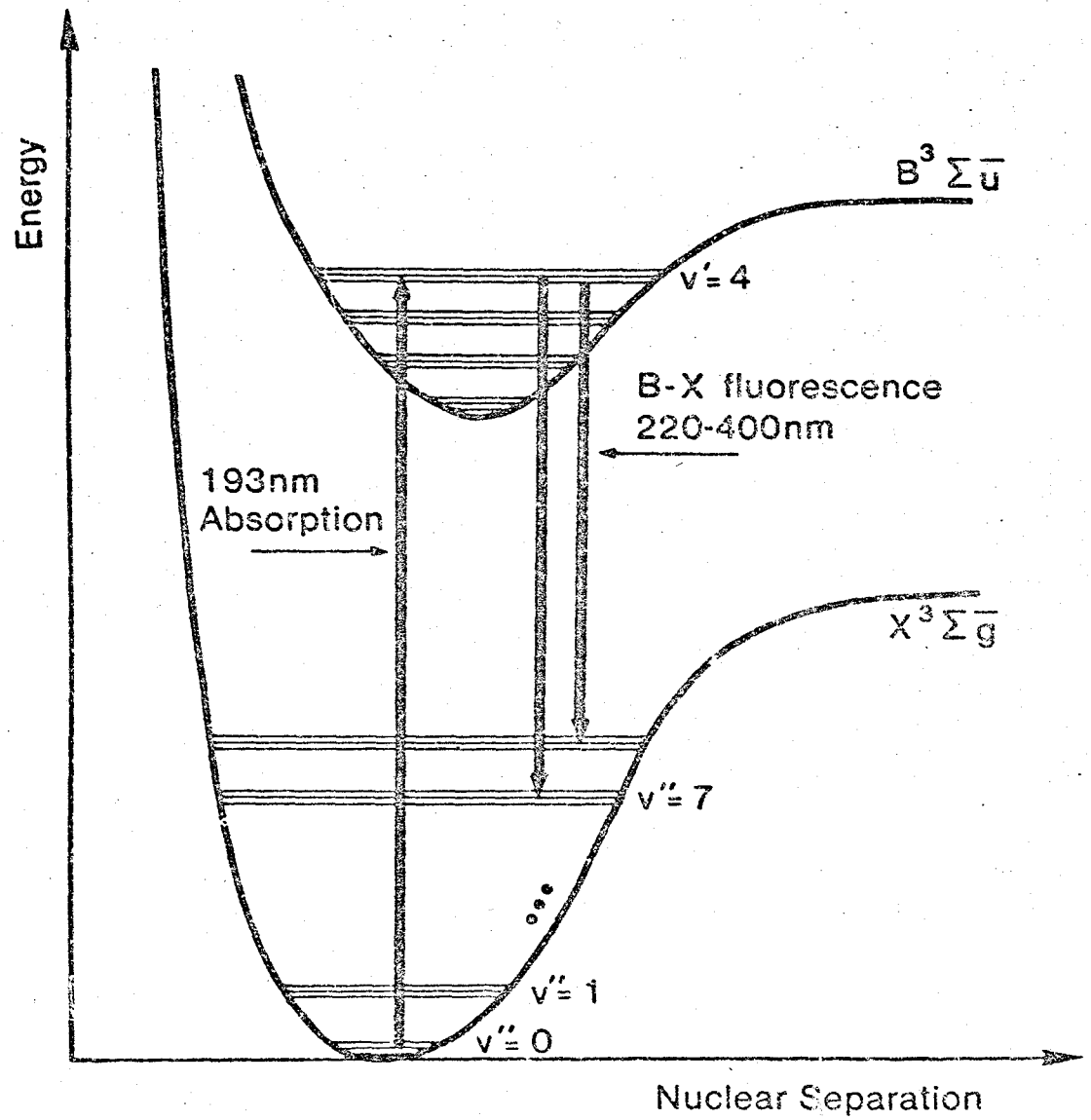

FIGURE 1. Energy levels and transitions of interest for the O_2 molecule.

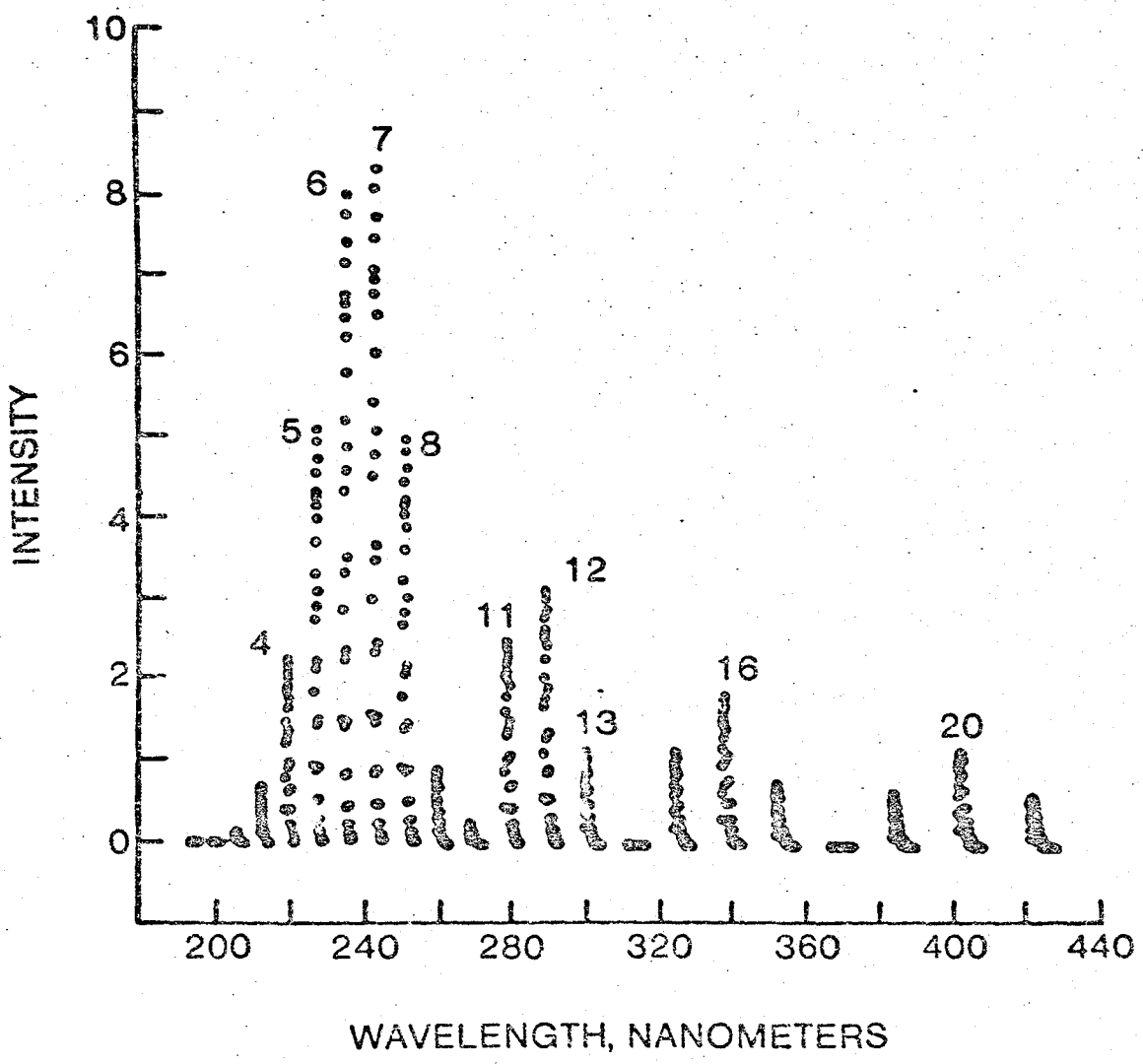

FIGURE 2. Spectrum of O_2 fluorescence produced by Schumann-Runge absorption near 193.3 nm.

a wavelength-dispersive optical receiver to sense the relative populations in the excited rotational states. However, further investigation revealed that predissociation of the excited B(v' = 4) level occurs within a few picoseconds, implying that those states do not equilibrate. For the same reasons, the fluorescence is very weak, (the quantum yield is 4×10^{-5}), and the losses associated with the dispersive receiver optics would seriously reduce the signal to noise ratio. The predissociation results in formation of two O_3 molecules for each absorbed photon at 193 nm, and O_3 has a very large, broad absorption near 260 nm. Therefore, some attention was given to the possibility of observing the O_3 produced by a tuned ArF laser excitation of the O_2 rotational states. However, the maximum O_3 concentration produced is of the order of 10^{14} cm^{-3}, and this must be detected in a 1 mm^3 volume (i.e., the optical path is 1 mm), giving an absorption of only 0.01%. A low pressure mercury discharge lamp can provide a reasonable S/N for detection near 254 nm, but even with parallel differential path detection we found that low level refractive variations in the laboratory air made it difficult to detect the presence of the O_3 in a 1 mm path. It appeared unlikely that the additional two orders of magnitude sensitivity needed for quantitative turbulence measurements could be realized with that approach. Similarly, fluorescence from O_3 or other products of the O_2 dissociation occur with very low yield and are more difficult to monitor than O_2 fluorescence. For these reasons we are led to consider the system in which rotational states of the ground X (v" = 0) level are probed selectively with the ArF laser, with O_2 fluorescence providing a signal proportional to the ground state

populations before excitation.

Given that the above method is chosen, there remain some system alternatives. In one configuration the same air volume is illuminated by two different ArF wavelengths in rapid succession, and the time-resolved fluorescence ratio permits separation of temperature information from density variations. Alternatively, one can use a single ArF wavelength and measure both fluorescence (primarily 220-260 nm) and Rayleigh scattered 193 nm light. The Rayleigh signal depends on the gas density while the fluorescence depends both on temperature and density, so that the two effects are easily separated. This latter method is less complicated and more accurate than the dual wavelength technique, but it cannot be employed with air samples heavily loaded with particulate matter. We have investigated both techniques experimentally, and the results are described below. Details of the O_2 spectroscopy have been published in Reference 1 and in papers cited therein, and the O_3 experiments have been described in interim progress reports (Grant NAG 2-104 September 1981-March 1982, April-September 1982, and October-June 1983). This report will, therefore, document other findings of this study.

2. ArF Laser

The Schumann-Runge absorptions of interest are the P and R branch overlapping pairs of lines:

P13/R15	192.9 nm
P15/R17	193.1 nm
P17/R19	193.3 nm
P19/R21	193.5 nm
P21/R23	193.7 nm
P23/R25	193.9 nm

The ArF laser output peaks near 193.5 nm, but with prismatic tuning optics it can supply sufficient energy (~1mJ) near 193.1 nm and 193.9 nm in linewidths about 0.1 nm (20 cm^{-1}). This provides for rotationally specific excitation, although the efficiency is not ideal because the O_2 absorption lines are only 3 cm^{-1} wide. The primary ArF laser characteristics of interest are the high single pass gain and short gain duration (~10 ns). The optical cavity used here is more than one meter long, so that light completes only about one round trip during the gain interval. Wavelengths selection techniques are less effective in this case than they would be in a device with lower gain and longer buildup time. The laser developed for this work employs a 1-meter discharge gain channel enclosed by CaF_2 windows, with two Brewster angle fused silica prisms and a total reflector at one end and a slit and uncoated fused silica etalon at the opposite end. The combination of prisms and slit proves wavelength selectivity; tuning is accomplished by adjusting the angle of the totally reflecting mirror. The configuration is shown in Figure 3. The tuning device cannot be very lossy (as a grating would be), because there is always nondispersed radiation generated in the gain channel traveling in the direction of the output etalon, and

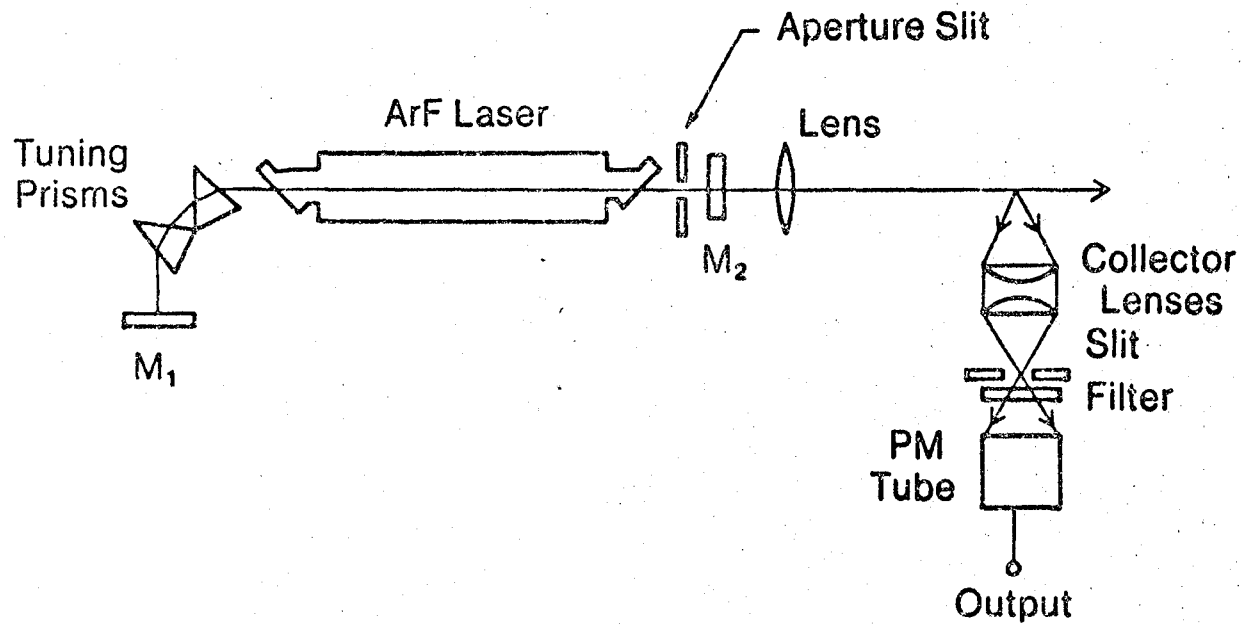

FIGURE 3. Schematic diagram of the optical system of the ArF laser used for fluorescence excitation. Tuning is accomplished by tilting the fully reflecting mirror M_1.

this broadband light competes with the energy returning from the tuning optics.

The laser is discharge pumped with ultraviolet preionization furnished by a spark plug array. Voltage is supplied by a Hipotronics Model 850-20 power supply which stores energy in a 50 nF capacitor. One end of this capacitor is switched to ground by a Tachisto Model 510 triggered spark gap, while the other is connected to a 20 nF array of barium titanate capacitors mounted directly above the cathode rail of the laser (see Figure 4). This provides a voltage that reaches -25kV in approximately 70 ns and then discharges into the channel in about 15 ns. The mechanical arrangement of these components is critical in achieving the necessary fast discharge. Four of the barium titanate capacitors return current to ground through an array of spark plug preionizers along one side of the discharge channel. Because this laser is to be used with prism and slit tuning optics the electrodes are narrower (~1.2 cm wide) than conventional lasers designed to produce a square gain region. With 30kV on the storage capacitor and 2 atmospheres total gas pressure the device emits 2-6 mJ in a 20 cm^{-1} linewidth. The gas mixture is approximately 10% Ar, 10% mixture of 5% F_2 in He, and 80% pure He, separately metered and monitored in a flowing system providing about 2 liter per minute longitudinal flow through the laser. The gas mixture was found to be critical for attaining high gain. After the flow rates were optimized experimentally, even a 10% change in one of the inlet components produced a large drop in output. The system flow was made as large as possible consistent with the laser body pressure and resistance in the 6mm stainless

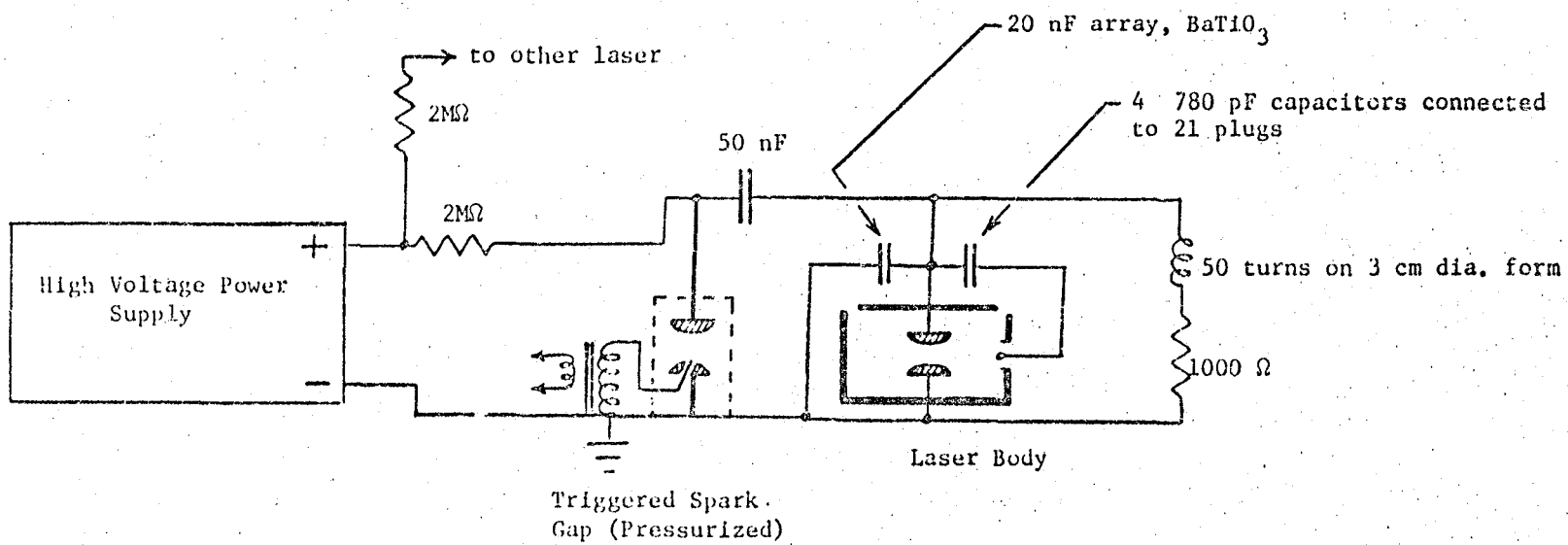

FIGURE 4. Laser electrical schematic diagram. Two lasers can be run in parallel with independent triggering.

steel tubing used to exhaust the gas.

A large number of experiments were carried out earlier in this program to improve the laser performance. Briefly, the results may be summarized as follows:

1. A 60 cm discharge channel produced much less (2 to 10 times) output energy and gain than the 100 cm channel under the best conditions.

2. Mesh electrodes, segmented and ballasted electrodes, and electrodes with imbedded corona wire preionization produced less output than smooth single-piece electrodes.

3. It was not possible to increase the duration of gain in the channel.

4. The optimum preionization source was a spark gap array (modified Champion L78 spark plugs) on one side of the discharge channel, driven by only a small fraction of the discharge current. Techniques which were successful with $He:N_2$ lasers proved quite unsuccessful with ArF.

Mechanically the laser body was constructed of a single piece of aluminum with a Teflon covered acrylic plastic lid sealed with a large Viton O-ring. The anode electrode rail and holes for the spark preionizer plugs were machined into the aluminum body. The cathode rail was suspended from the plastic lid and attached to the capacitor array by a row of feedthroughs. No recirculating blower was used to move the gas in the body, although inclusion of such a device probably would have improved the laser performance.

Two identical laser bodies were constructed for the dual wavelength experiments. We found that they could be changed at repetition rates up to a few Hz from a single DC source with ballast resistance of about 2MΩ between the source and the energy storage capacitors. Trigger jitter was much less than one microsecond with the spark gap pressure adjusted properly. The entire laser and high

voltage system was enclosed in an aluminum box for shielding. Additional boxes with feedthroughs at each end permitted us to evacuate and backfill the optical paths with N_2. A purged tube carried the laser beams to the experimental table. The laser electronic system was isolated from the laboratory voltage source by a large isolation transformer to reduce interference in the receiver and computer.

Optical Receiver

Detection of the O_2 fluorescence, which is concentrated in the 220-260 nm region, as well as monitoring of scattered 193 nm energy, is easily done using bialkali photomultiplier tubes with fused silica windows. We used Hamamatsu type R292 and R760 detectors in this work. For fluorescence measurements it is necessary to eliminate 193 nm radiation (without introducing additional fluorescence) while passing 220 nm and longer wavelengths. We found that filters of this type are difficult to obtain. Several commercially available filter glasses were tested, and we found that their short wavelength characteristics were not as indicated in the literature. Alkali halide crystals were also evaluated. Samples of 6 mm thick KBr transmitted 0.1% at 193 nm, 45% at 220 nm, 60% at 240 nm, and above 70% beyond 270 nm. Sodium chloride passed 1% of the 193 nm signal, more than 70% at 225 nm, and about 80% beyond 250 nm. Both materials are easily degraded by laboratory humidity. The most successful filters we have found are crystal calcite ($CaCO_3$) and multilayer dielectric mirrors (narrowband 193 nm high reflectors) deposited on

both sides of a fused silica substrate. The multilayer filter passed about 0.1% of the 193 nm energy and transmitted more than 70% of the fluorescence. Our calcite sample with a 1 cm thickness blocked essentially all the 193 nm radiation and about half the fluorescence. This sample generated very weak fluorescence near 600 nm, while the mirrors show slightly greater amounts of blue-white fluorescence from the coatings and the substrate. In general the coated filter is more appropriate when there is not too much 193 nm background and the fluorescence is weak, while the calcite works better in situations where attenuation at 193 nm is most important.

In this work we employed a fused silica collecting lens of 25 mm aperture and 50 mm working distance. The fluorescence was imaged onto a slit in front of the filter and phototube so that a 1 mm path length along the laser beam axis was selected. For experiments requiring a greater working distance or a spatial resolution better than about a millimeter, this approach probably is not practical. For large working distances an all-reflective optical system similar to the Schwartzchild microscope objective can be used (see Figure 5). In this system the spherical aberrations of concave and convex mirrors compensate each other. Early in this work we designed (see Reference 2) and constructed such a collector with a 30 cm working distance, F/3 collection angle, and sample resolution better than 45 micrometers. Although such systems are bulky they provide a way to collect broadband UV efficiently and with the great advantage that the masking aperture alignment and focusing can be done exactly with visible light. Care must be taken to obtain highly reflecting UV coatings on substrates more than a few cm in diameter.

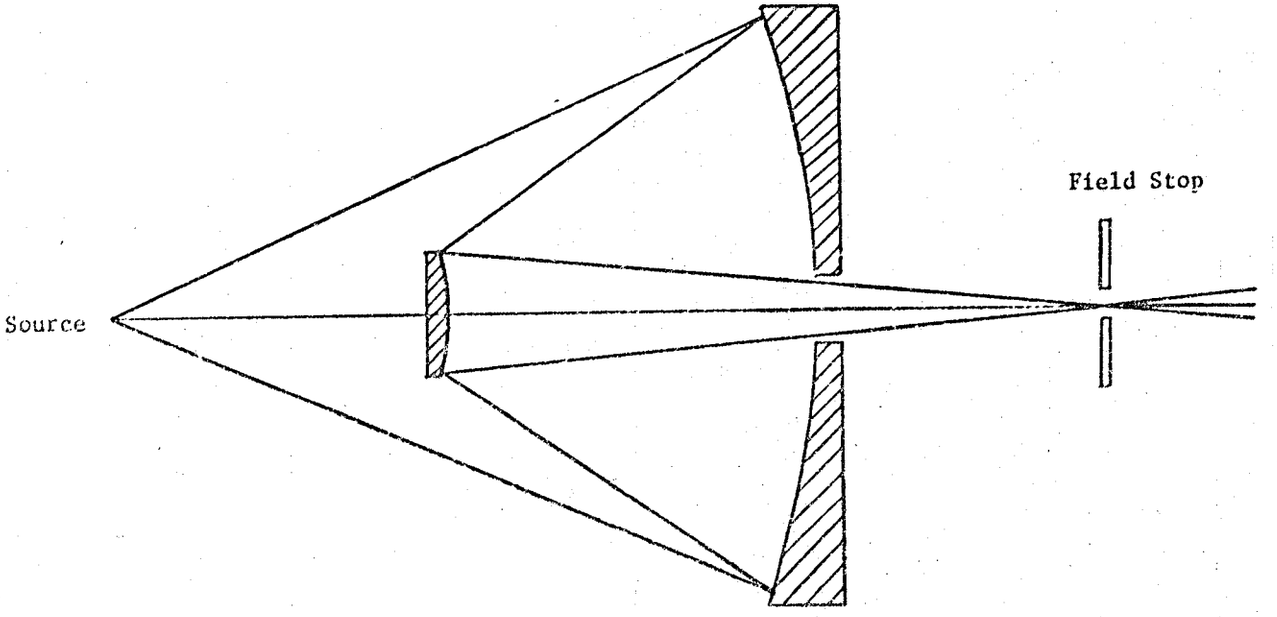

FIGURE 5. Reflecting collector for use with large working distances. Both mirror surfaces are spherical. Numerical apertures up to 0.6 are practical.

The number of dynodes used in the phototubes was selected to provide an output current within the maximum rating for the tube, i.e., a few tens of microamperes. For the 10 ns optical pulse duration this corresponds to an output charge slightly greater than 10^{-13} coulomb. Typically, the cathode charge was in the 10^{-14} - 10^{-15} coulomb range. To avoid problems with electromagnetic interference the output charge was stored on the coaxial cable (~100 pF) connecting the phototube to its video amplifier. A potential step of about $Q/C = 10^{-3}$ volts is therefore presented to the amplifier input. Since potentials in the one-volt range are needed for signal processing by the digitizer and computer, the required amplifier voltage gain is about 1000. In experiments with two lasers at different wavelengths, the pulses must be time resolved. This requires that the risetimes of the voltage steps should be about a microsecond. The circuit developed for this purpose is shown in Figure 6.

The output voltages were displayed and processed in either of two ways. The most direct way, useful when only one laser is employed, is to apply the fluorescence detector voltage to the Y axis and the laser power or Rayleigh scattering voltage to the X axis of a storage oscilloscope. With beam parameters correctly adjusted each laser pulse produces a small dot on the display, the angle of the dot position relative to the axes representing the efficiency of the fluorescence. As the sample density or temperature changes and more laser samples are collected, a pattern is formed on the screen. This is easily recorded in a photograph for further processing. A single streak of dots represents constant sample conditions with the laser

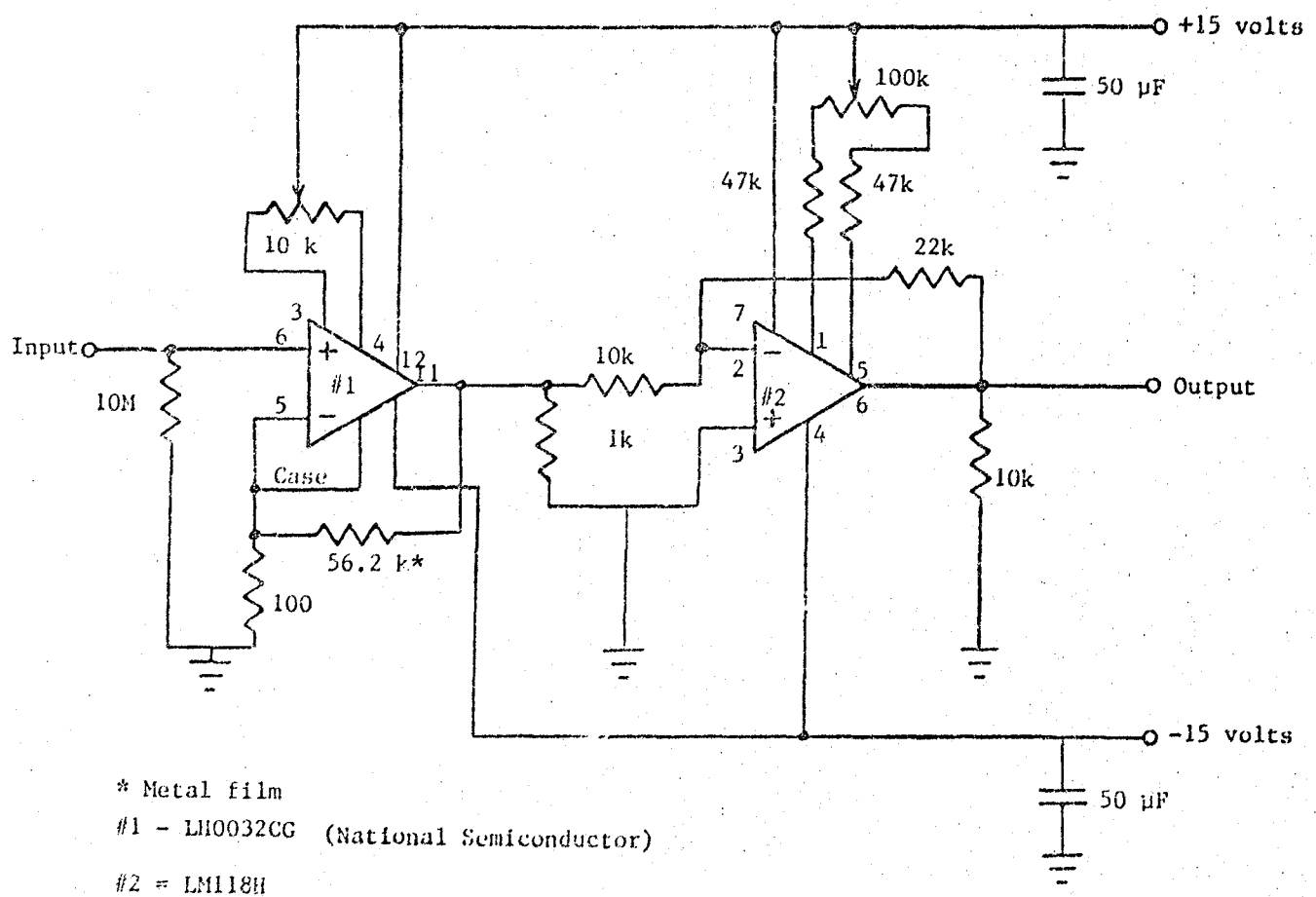

FIGURE 6. Video amplifier circuit schematic diagram. The ±15 volt source is a battery package mounted inside the amplifier enclosure to reduce laser interference.

power fluctuating. A two dimensional pattern indicates in polar form any sample changes or noise (angle) or laser fluctuations (radius) from the X-Y origin. Figure 7 shows an example of such a data set.

For dual wavelength experiments with two lasers a more complex processor is needed. For this purpose we developed a two channel, 8-bit digitizer which samples the waveforms at 10^7 per second, stores the values in a memory, and displays the sampled waveform. The voltages are double steps, one for each laser in each detector channel, and the two channels permit fluorescence and a second variable (e.g., laser power or Rayleigh scattering) to be monitored simultaneously. The system uses pairs of TRW Model TDC 1007J A/D converters and TDC 1030 first-in first-out memories for storing 64 pairs of 8-bit numbers. The sample rate is adjustable and typically was set at 10 MHz. The sample values are transferred to a Commodore 64 computer which reconstructs the waveform on its monitor screen. A movable cursor permits specific points on the waveform to be evaluated numerically and printed. Ratios, differences, and other functions are easily taken, and the waveforms themselves can be recorded in hard copy form (see Figure 8).

Although this data collection procedure is slower than collecting points automatically on the storage scope screen, it does permit the collection of data corrupted by interference from the laser, and it facilitates statistical processing, such as computation of standard deviations.

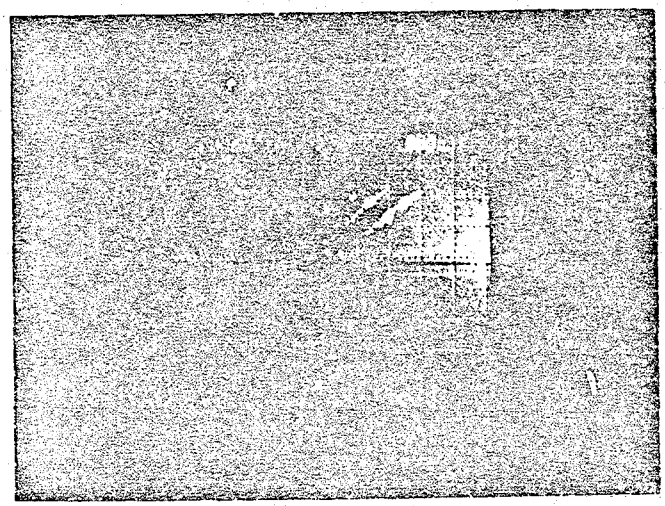

FIGURE 7. Oxygen fluorescence (vertical) vs. Rayleigh scattered laser energy tuned to P19/R21 for air at 29.5°C (lower line) and at 58.5°C (upper line). Each pulse is represented by one dot.

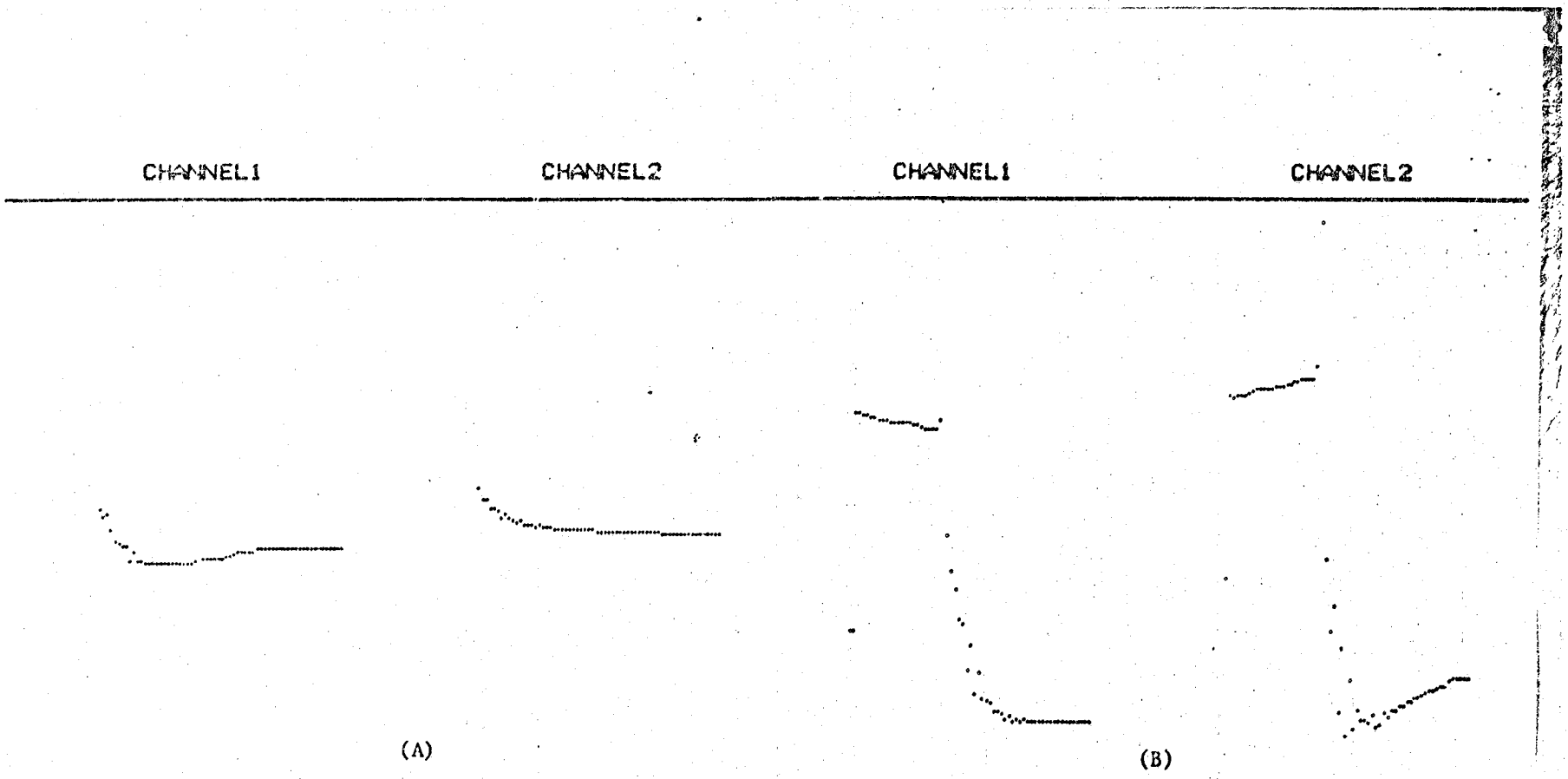

FIGURE 8. Output waveforms from the digitizer system with single pulse excitation (A) and double pulse excitation (B). Note the presence of interference on the Channel 2 waveform in (B). Increasing signal is downward and zero signal is the dark line at the top.

3. Experimental Results

The apparatus used in the experiments is shown schematically in Figure 9. A photoacoustic cell which could be filled with O_2, N_2, or air was used to verify the nature of the laser absorption spectrum independently of optical fluorescence methods. Also a 5th order diffraction grating and fluorescent screen displayed the position of the laser wavelengths relative to the atmospheric absorption lines. The reference signal could be derived either from 193 nm scattering from the gas sample (Rayleigh reference) or from the laser power scattered from one of the lens surfaces (laser reference), simply by aiming the unfiltered phototube assembly in different directions. A Scientech Model 360 power meter was used to ensure that the laser energy was in the 1-2 mJ range when tuned to line center, which is near the P19/R21 absorption feature of O_2.

From basic considerations we expect that at temperature T the fraction of O_2 molecules in the J'th rotational ground state should be

$$n(J)/n_0 = (2J+1)(a/T)\ \exp[-J(J+1)\ a/T] \qquad (1)$$

where $a = hc\ B_v/k = 2.0686$ degrees Kelvin. We also know that the total number density n_0 is proportional to p/kT, where p = pressure and k is Boltzmann's constant. In addition, since P and R branch transitions occur in pairs, we can associate the number J with the P branch alone and write the detected fluorescence intensity as

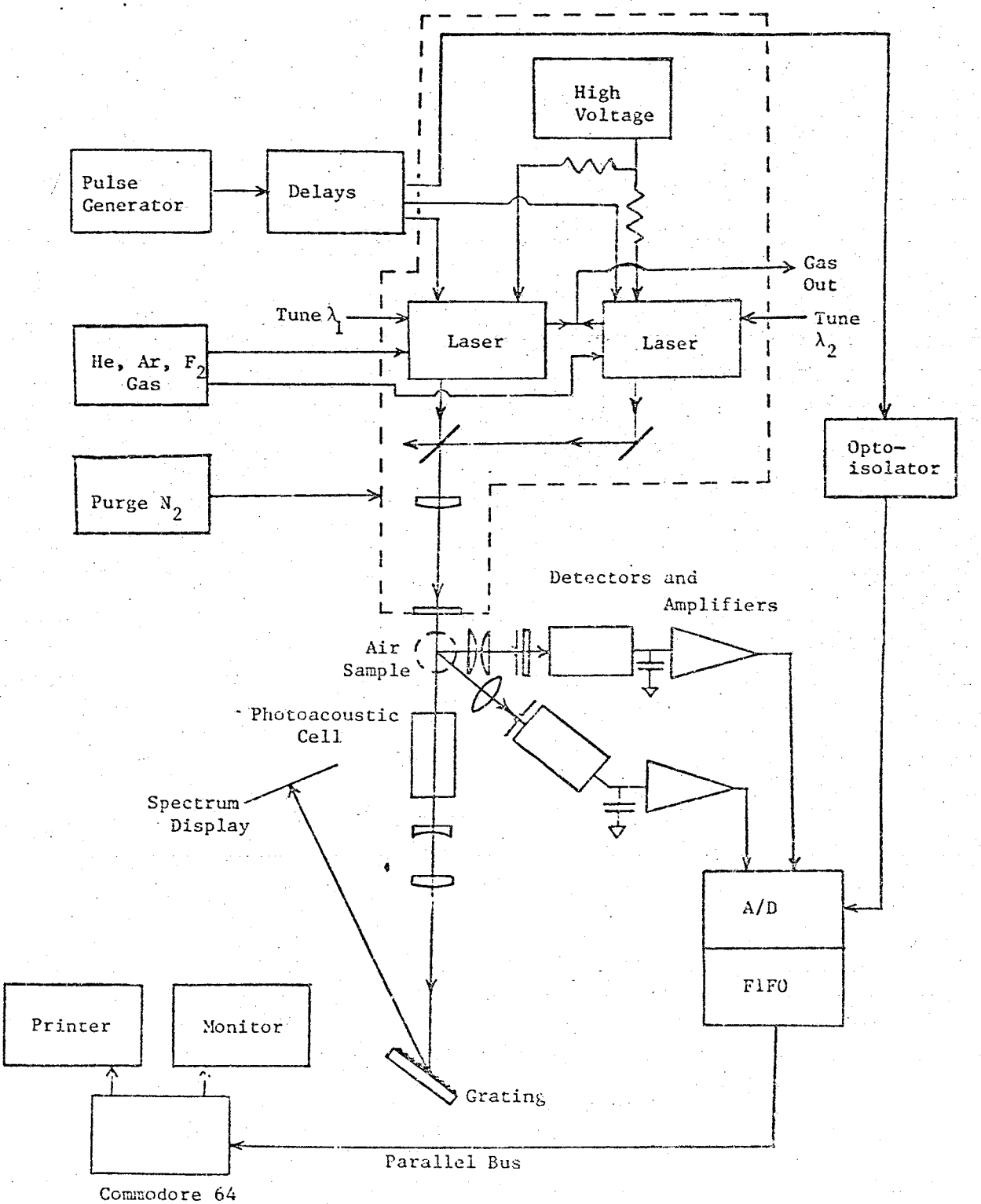

FIGURE 9. Experimental apparatus.

$$I(J, T, p, E) = (AEp/T^2)\ \{(2J+1)\ \exp\ [-J(J+1)\ a/T] + (2J+3)\ \exp\ [-(J+1)(J+2)\ a/T]\} \quad (2)$$

where E is the laser energy exciting the P(J)/R(J+2) transition and A is a constant of proportionality.

If the fluctuations in T and n produce small changes in I, then the appropriate relation is

$$\Delta I/I = (\Delta T/T)\ \{[J(J+1) + (J+2)\ (J+3)]\ (a/2T) - 1\} + \Delta n/n_0 \quad (3)$$

For the special case of air at constant pressure we have

$$(\Delta I/I)_p = (\Delta T/T)\ \{[J(J+1) + (J+2)(J+3)]\ (a/2T) - 2\} \quad (4)$$

There is also the inverse problem, in which we measure $\Delta I/I$ at 2 laser wavelengths (2 J values) and we want to recover $\Delta T/T$ and $\Delta n/n_0$. In that case a direct application of Cramer's Rule gives

$$\Delta T/T = [C_1(\Delta I/I)_2 - C_2\ (\Delta I/I)_1]/(C_1C_4 - C_2\ C_3) \quad (5)$$

$$\Delta n/n_0 = [C_4(\Delta I/I)_1 - C_3(\Delta I/I)_2]/(C_1C_4 - C_2\ C_3) \quad (6)$$

where $C_1 = C_2 = 1$ in this case and

$$C_3 = [J_1(J_1+1) + (J_1+2)(J_1+3)]\ (a/2T) - 1 \quad (7)$$

$$C_4 = [J_2(J_2+1) + (J_2+2)(J_2+3)]\ (a/2T) - 1 \qquad (8)$$

The goal of the experiments is to verify the basic relations above and to determine the accuracy with which the measurements can be made under practical conditions.

A fundamental question is the sensitivity of the system to changes in the fluorescence, after the laser power fluctuations are normalized out. With a single ArF laser tuned to the P19/R21 line of room temperature laboratory air we have estimated the accuracy of the X-Y display method with fluorescence pulses plotted against laser power. A typical result is Figure 10, for which the peak spread is $\pm 2\%$ for a large number of samples. Alternatively, we have used the digitizer to sample the fluorescence/laser energy ratio for the same line with the air temperature and density held constant. The computed standard deviation for this ratio is 1.8%. These numbers are reasonable since each detector channel produced about 10^4 cathode electrons per pulse in these experiments.

Using a hot air blower and thermistor thermometer to move air at constant pressure through the laser beam, we were able to verify the temperature coefficients for the fluorescence over the 20°C to 60°C range. For example, by comparing the fluorescence signal to Rayleigh scattered signal for air at one atmosphere pressure at two temperatures, 325°K and 296°K, we obtain the following:

Line	$\frac{\text{(Fluorescence/Rayleigh) at 325K}}{\text{(Fluorescence/Rayleigh) at 296K}}$	
	Experiment	Theory
P17/R19	1.128	1.114
P23/R25	1.302	1.302

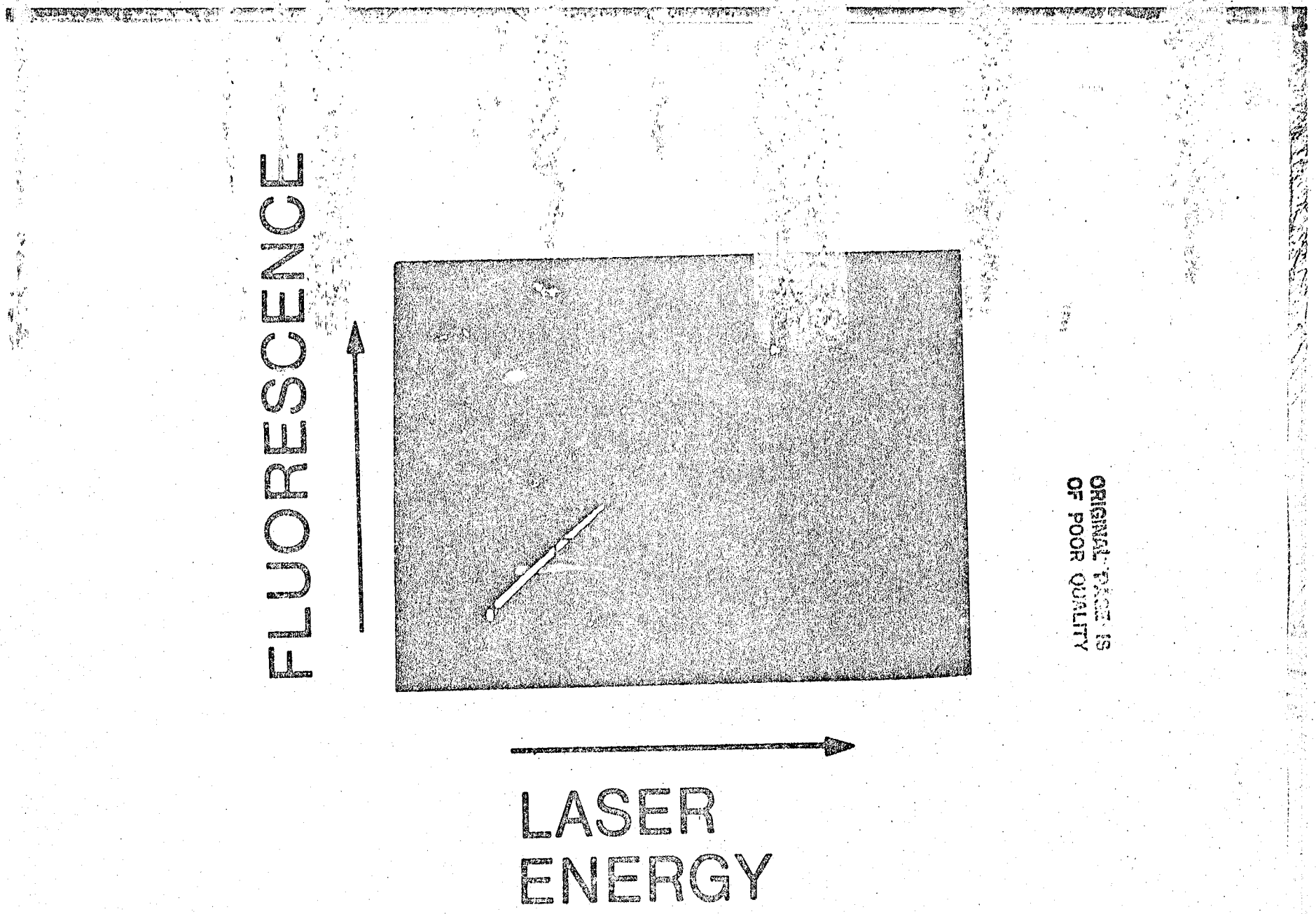

FIGURE 10. XY display of oxygen fluorescence vs. laser energy tuned to the P19/R21 absorption wavelength. Vertical thickness of the trace indicates the noise level.

End of Document